Available online at www.sciencedirect.com
SCIENCE DIRECT
Polymer 46 (2005) 5103–5117
polymer
www.elsevier.com/locate/polymer

Uniaxial deformation of an elastomer nanocomposite containing modified carbon nanofibers by in situ synchrotron X-ray diffraction

Antonis Kelarakis, Kyunghwan Yoon, Igors Sics, Rajesh H. Somani, Benjamin S. Hsiao*, Benjamin Chu**

Department of Chemistry, Stony Brook University, Stony Brook, NY 11794-3400, USA

Received 12 February 2005; received in revised form 25 April 2005; accepted 25 April 2005

Abstract

Structure and property of a nanocomposite consisting of modified carbon nanofibers (MCNFs), homogenously dispersed in an elastomeric ethylene/propylene (EP) random copolymer (84.3 wt% P) matrix, were studied by in situ synchrotron X-ray diffraction during uniaxial deformation. The MCNF acted as a nucleating agent for crystallization of the α-form of isotactic polypropylene (iPP) in the matrix. During deformation at room temperature, strain-induced crystallization took place, while the transformation from the γ phase to α phase also occurred for both unfilled and 10 wt% MCNF-filled samples. The tensile strength of the filled material was consistently higher than that of pure copolymer. However, when compared with pure copolymer, the highly stretched nanocomposite exhibited a higher amount of unoriented crystals, a lower degree of crystal orientation and a higher amount of γ crystals. This behavior indicated that polymer crystals in the filled nanocomposite experienced a reduced load, suggesting an effective load transfer from the matrix to MCNFs. At elevated temperatures, the presence of MCNFs resulted in a thermally stable physically cross-linked network, which facilitated strain-induced crystallization and led to a remarkable improvement in the mechanical properties. For example, the toughness of the 10 wt% nanocomposite was found to increase by a factor of 150 times at 55 °C.

Keywords: Ethylene–propylene elastomer; Carbon nanofiber; Nanocomposite

1. Introduction

The growing research interest for carbon nanotubes (CNTs) and carbon nanofibers (CNFs) in both academia and industry reflects the great potential of these new carbon allotropes for a wide spectra of applications [1], including the development of fire retardant additives [2], high-strength composites [3,4], conducting and semi-conducting materials [5], energy storage devices and electro-mechanical actuators [6], just to name a few. The unique properties of these materials were realized by the scientific community soon after their introduction [7]. However, despite considerable efforts that have been directed towards the goal of coupling the fascinating properties of carbon nanofillers with conventional polymers, several aspects of nanocomposites remain unclear.

In mechanical reinforcements, major issues are the homogenous dispersion of nanofillers in the polymeric matrix and the development of chemical bonding or strong interactions at the nanofiller–matrix interface [8]. Both these conditions must be fulfilled in order to promote an efficient load transfer across the nanofiller–matrix interface and, thereby, improve the strength of the composite. To address these issues, two general approaches have been proposed. The first approach [9,10] considers the wrapping of nanofillers by a high molecular weight polymer, avoiding any chemical modification of the surface. The second approach [11–14] focuses on the covalent attachment of functional groups on the graphitic sidewalls. The latter route has been widely explored in order to promote the dispersion of nanofillers into polymeric matrices and, thus, optimize the performance of the nanocomposites.

The main objective of this work is to investigate the

* Corresponding authors. Tel.: +1 631 632 7793; fax: +1 631 632 6518.
** Tel.: +1 631 632 7928; fax: +1 631 632 6518.
E-mail addresses: bhsiao@notes.cc.sunysb.edu (B.S. Hsiao), bchu@notes.cc.sunysb.edu (B. Chu).

0032-3861/$ - see front matter © 2005 Elsevier Ltd. All rights reserved.
doi:10.1016/j.polymer.2005.04.057

effects of the surface modified carbon nanofiber (MCNF) on the deformation mechanism of an elastomeric nanocomposite. A random ethylene/propylene (EP) copolymer with 84.3 wt% P was chosen as the elastomeric polymeric matrix. The tensile properties of this thermoplastic copolymer have been reported by us previously [15]. The EP copolymer, being recently commercialized [16], is easy to process and fabricate, in contrast with natural rubber and EPDM (ethylene–propylene diene monomer) rubber, and can retain its elastic performance at room temperatures. The hard segment of the copolymer consists of isotactic polypropylene (iPP) crystals within the continuum of the amorphous domain. These crystals act as physical cross-linkers, leading to high viscosities at room temperatures, but they can be melted at reasonable temperatures facilitating the processing of this material.

When MCNFs are incorporated into this copolymer, they act as secondary cross-linkers and can significantly modify the mechanical properties of the nanocomposites. The MCNFs used in this study were chemically grafted with short polypropylene chains and were solution blended in xylene with the polymeric matrix. The resulting nanocomposite appeared to be homogenous by scanning electron microscopy (SEM) examination, indicating strong van der Waals interactions between the MCNFs and the polymer chains. Although the reported tensile strengths of CNT are in the range of a 100 GPa and the Young's moduli are in the TPa range [8], the corresponding values for CNFs are considerably lower [17]. However, CNFs are more easily functionalized due to the layer edge defects by the presence of tilted graphite layers to the CNF axis [18].

Several reports focusing on the mechanical reinforcement of polypropylene materials with CNFs [19–22] and CNTs [14,23] have appeared in the literature. CNF and CNT reinforced elastomers [24,25] have also been studied to some extent. However, the deformation mechanism of such nanocomposites has not yet been fully understood. In order to gain insightful information towards this subject, we have performed in situ synchrotron wide-angle X-ray diffraction (WAXD) studies during uniaxial deformation of MCNF-reinforced elastomeric nanocomposites. Time-resolved WAXD patterns for both pure copolymer and nanocomposites were obtained during stretching experiments at room temperature, as well as at elevated temperature (55 °C). The study was focused on: (1) the crystallinity development and the structural changes during stretching of the nanocomposite, and (2) the effect of temperature on the deformation mechanism.

2. Experimental section

2.1. Materials and sample preparation

The EP random copolymer was provided by the ExxonMobil Chemical Company. It is a member of the commercial 'Vistamaxx' specialty elastomers [16]. The copolymer was synthesized with the aid of the metallocene catalyst. It had 84.3 wt% propylene (P) content, with $M_n = 9.6\times10^4$ g/mol and $M_w = 1.7\times10^5$ g/mol. Carbon nanofibers (Pyrograf III, PR-24-HHT) were purchased from Applied Sciences. Their diameters varied from 60 to 150 nm and the estimated length was between 30 and 100 μm. This product was used without further purification.

A polypropylene-graft-maleic anhydride polymer ($M_n =$ 3900 g/mol, $M_w = 9100$ g/mol, acid number = 47 mg KOH/g) was purchased from Aldrich and was used for attachment to the sidewalls of CNFs. Other chemical agents used in the grafting reaction included: xylene (Fischer, HPLC grade), dichlorobenzene (Aldrich), methanol (Fischer, HPLC grade), ethanol (abs. Aldrich), sodium borohydride (Aldrich), sulfuric acid (conc. Aldrich), nitric acid (conc. Aldrich), sodium hydroxide (Fischer), and water (Milli-Q). All chemicals were used without further purification. The chosen chemical grafting scheme of the CNFs is illustrated in Scheme 1, and the detailed procedures are as follows.

One gram of CNFs was dispersed in 200 ml of a sulfuric acid/nitric acid mixture (volume ratio = 3:1) and the dispersion was heated up to 60 °C for 2 h under stirring [26]. The oxidized CNFs were filtered and washed first with water (until the filtrate became neutral), and then with acetone (250 ml). The recovered powder was dried in an oven at 80 °C overnight before further modification. The product produced after the oxidation step was titrated by sodium bicarbonate. Based on the titration method, the concentration of carboxylic groups in the product was 0.55 mmol/g (in the untreated CNF, no detectable value of carboxylic acid groups could be measured). One gram of the carboxylated CNFs was dispersed in 200 ml of ethanol. Sodium borohydride (75.66 mg) was then added and the dispersion was refluxed at 80 °C for 5 h [27]. After being cooled down, the mixture was filtered and washed with 9 M sulfuric acid. The filtered powder was rinsed with water (until pH ~ 7) and acetone. Using the Haddon procedure [28], we also determined the concentration of the acidic groups by sodium hydroxide titration (~0.94 mmol/g) and the concentration of the carboxylic groups by sodium bicarbonate titration. After the final step, no detectable concentration of carboxylic groups could be measured, indicating the complete reduction of –COOH to –OH groups.

One gram of hydroxylated CNF was dispersed in 200 ml dichlorobenzene and a polypropylene-graft-maleic anhydride polymer was added to the dispersion and then heated up to 120 °C with stirring for 5 h [29]. The solution was filtered and washed with hot dichlorobenzene (~500 ml). The recovered powder was put into the soxhlet extraction apparatus and refluxed for several days with cyclohexane until it reached a constant weight. It was then dried in a vacuum oven at 80 °C for 1 day. Polypropylene-grafted CNFs (~0.1 g in the case of 10 wt% nanocomposite) were

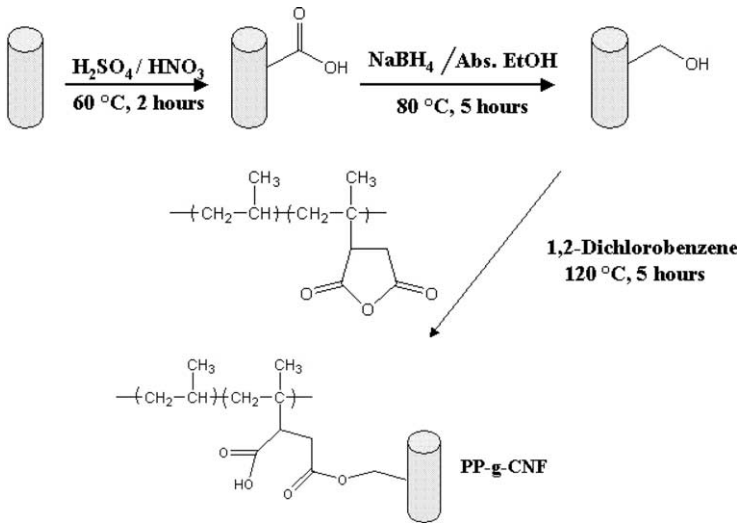

Scheme 1. Schematic representation of the chemical treatment used for functionalization of CNFs.

dispersed in xylene (440 ml) by using an ultrasonicator for 30 min. The EP copolymer was added to the solution at 120 °C and stirred for 2 h. The mixture was precipitated into cold methanol (~2 l), filtered, and dried at 90 °C in vacuum for a day.

The dried polypropylene-grafted CNFs (~10 mg) were characterized by thermal gravimetric analysis (TGA). The samples were measured under air atmosphere at a heating rate of 20 °C/min. In particular, TGA curves were obtained for: (1) the untreated CNFs, (2) the polypropylene-grafted CNFs (termed MCNF hereafter), and (3) the pure PP-*g*-MAH compound. A comparison of TGA curves (1) and (2) showed that the concentration of PP-*g*-MAH in the MCNFs was close to 20 wt%. The thermal degradation of the attached PP-*g*-MAH in MCNFs was shifted to higher temperatures than that in pure PP-*g*-MAH, indicating the presence of covalent bonding between PP-*g*-MAH and CNFs. Given that MCNFs can be well dispersed in several solvents (e.g. hot xylene), the possibility of significant cross-linking during the grafting step can be excluded. If that were the case, aggregation of MCNFs would be observed in the SEM images of the fractured nanocomposites, which was not seen.

2.2. Instrumentation and experimental procedures

In situ time-resolved wide angle X-ray diffraction (WAXD) experiments were performed at the X27C Advanced Polymers beamline in the National Synchrotron Light Source (NSLS), Brookhaven National Laboratory (BNL), USA. The wavelength of the synchrotron radiation was 0.1371 nm. Two-dimensional (2D) WAXD patterns were collected using a MAR CCD detector (MARUSA, Inc.) with a resolution of 1024×1024 pixels (pixel size = 158.44 μm). The acquisition time for each image was 30 s. The sample to detector distance was 111.7 mm. The diffraction angle was calibrated by using an Al_2O_3 standard. The 2D WAXD patterns were corrected for the incident beam intensity fluctuations, as well as air and instrument scattering.

Stretching of the sample was accomplished by using a modified Instron 4442 tensile apparatus, equipped with a temperature chamber. The tensile machine allowed symmetric deformation of the sample at a constant rate of 10 mm/min and the detection spot on the sample remained fixed in space. The samples were put into a mold and melt-pressed at 150 °C under a pressure of 4000 kg/m^2 for 3 min. The molded samples were quenched in ice water. The samples were cut into a dumbbell shape and had an original length of 25 or 10 mm, depending on the desired maximum elongation. The strain at time t was calculated as $(l-l_0)/l_0$, where l is the length of the sample at time t and l_0 is the original length of the sample.

A dynamic mechanical analyzer (DMA) Rheometric Scientific, model RSA II) was used to measure the tensile modulus, of the unfilled and 10 wt% filled sample. The measurements were carried out from room temperature to 80 °C, and at a fixed frequency of 10 rad/s (within the linear region of viscoelasticity). It was performed in a tensile mode, using a heating rate of 2 °C/min. The samples were cut in rectangular strips. The morphology of the CNF in EP was determined by SEM. For this experiment, the sample was immersed in liquid nitrogen for 3 min and then cut by a razor blade to prevent deformation of the cross-section area. SEM images were obtained using a Leo 1550 microscope operated at an acceleration voltage of 10 kV. The sample was subject to gold coating in order to reduce the charging effects.

3. WAXD data analysis

In order to convert the 2D flat-plate WAXD images into the undistorted geometry in reciprocal space, we followed the 'Fraser correction' procedure [30]. To estimate the

oriented and unoriented components of the polymer and the degree of nanofiller orientation, we used the 'halo method' [31] in the Polar software (Stonybrook Technology and Applied Research). The basic assumption of this method is that the azimuthally independent component of the total scattered intensity is directly proportional to the unoriented portion of the sample. Therefore, the oriented portion of the sample can be obtained by subtracting the azimuthally independent component from the total scattered intensity. For each azimuthal scan, the minimum value of the intensity is considered as the intensity that arises from the unoriented scatterers. The isotropic contribution thus obtained was subtracted from the 2D WAXD pattern, yielding the contribution of the oriented scatterers.

The deconvolution of the 1D WAXD intensity profiles into the amorphous halo and lD crystalline peaks was done by the peak fit routine in the Peak Fit program. The shape of the amorphous peak was obtained from the WAXD pattern of the sample in its molten state, which was fitted with three Gaussian functions. Additional Gaussian functions were used to fit the crystalline peaks. This internal fitting procedure provided the crystallinity index of the sample. We favor the term crystallinity index rather than crystallinity, given that the percentage of crystallinity of a sample determined by different techniques may be different. The total crystallinity index, X_C^T, can be estimated by using the simple equation

$$X_C^T = 100\% - X_A^T \quad (1)$$

where X_A^T represents the percentage of the amorphous halo. Similar peak fit procedures were used to deconvolute the intensity profiles of the oriented and unoriented components in order to determine the corresponding oriented and unoriented crystallinity indices, X_C^O and X_C^U, respectively.

4. Results

4.1. CNF dispersion and nanocomposite mechanical properties

Fig. 1 shows a typical SEM image of 10 wt% MCNF-EP nanocomposite, taken along the cross-section of the prepared sample, in the undeformed state at room temperature. SEM images showed that the chemical functionalization of CNFs was effective, where MCNFs appeared to be uniformly dispersed in the polymeric matrix without appreciable aggregation. The homogenous dispersion of MCNFs as well as the efficient MCNF-polymer wetting and adhesion have led to substantially improved mechanical properties, as seen in the tensile measurements. Fig. 2(a) shows the stress–strain curves of pure copolymer and 1, 10 and 20 wt% nanocomposites during extension (with strain up to 6) and subsequent retraction to zero stress. For clarity, the retraction process for the 1 wt% sample was not presented. None of the samples exhibited a clear yield behavior; instead, they all showed a decrease in the stress rate at low strains. The increase in the tensile strength was apparent even for the 1 wt% sample and became more pronounced at higher nanofiller loadings. The strength of the 20 wt% sample was not much higher in comparison to that of the 10 wt% sample, indicating a saturation point at high filler loading. Based on results in Fig. 2(a), it is clear that a moderate level of filler loading, up to ~10 wt%, should provide a significant increase in the tensile modulus for the tested nanocomposites. Hence, further tensile experiments were focused on the 10 wt% sample.

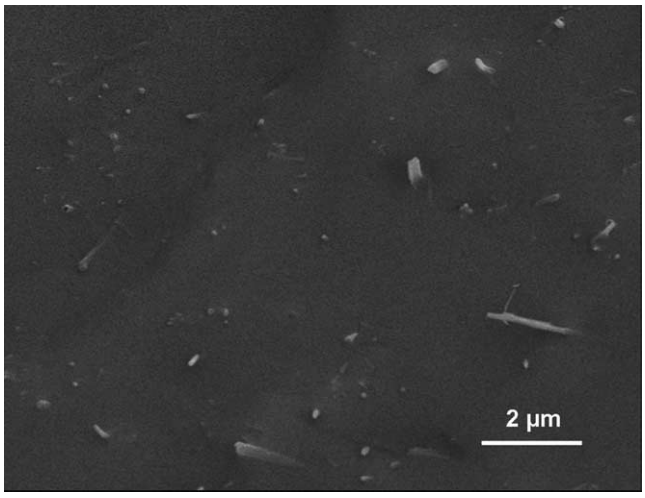

Fig. 1. SEM image of a 10 wt% MCNF–EP nanocomposite, taken along cross-section of the prepared sample, in the undeformed state at room temperature.

It is interesting to note that the stress recovery behavior of the polymer was also changed due to the presence of MCNFs (inset of Fig. 2(a)). During the retraction process, zero stress values were reached at higher strains in the filled samples, indicating that the elastic recovery was lessened in the nanocomposite. An additional amount of energy was, therefore, stored and could be released when the material was processed in an appropriate way; for example, by means of controlled heating [25]. The promising properties of these carbon nanocomposites could be utilized for the development of shape memory materials [32,33].

Dynamical mechanical analysis (DMA) was commonly used for the study of nanocomposite materials [21]. Temperature scans of the tensile modulus of pure copolymer and the 10 wt% filled sample are demonstrated in Fig. 2(b). The higher values of tensile modulus at all measured temperatures were observed for the filled sample, which is a highly desired property for nanocomposites. The advanced mechanical performance of the nanocomposites at high temperatures can be used in applications such as the development of fire retardant materials [2].

4.2. Nucleating effect of MCNF to EP copolymer matrix

The circularly averaged WAXD intensity profile for the

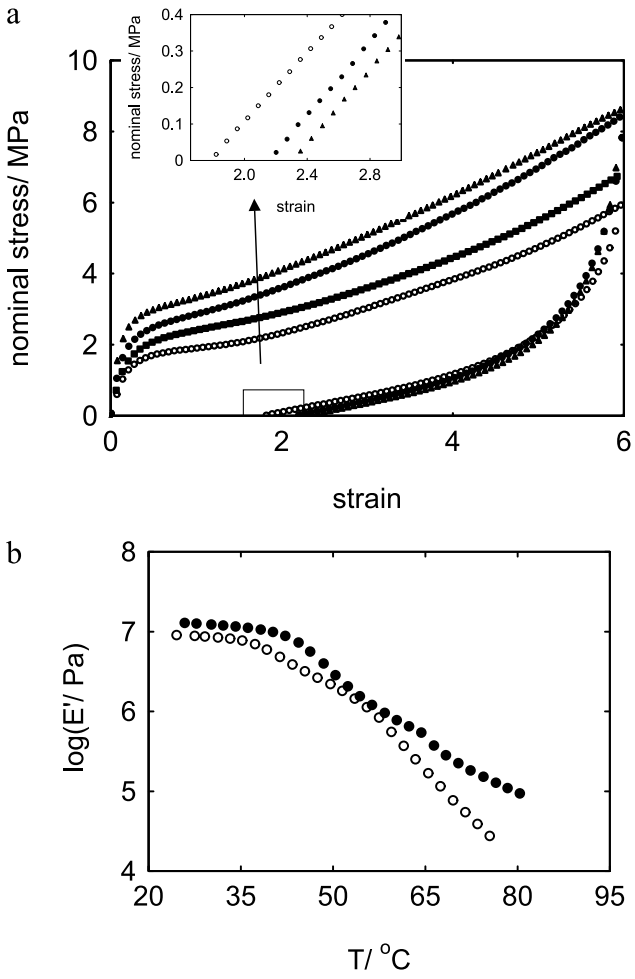

Fig. 2. (a) Stress–strain curves of the pure copolymer (unfilled circles) and 1 (squares), 10 (filled circles) and 20 wt% (triangles) MCNF-EP nanocomposites at room temperature. The inset shows the final stage of the retraction process. (b) Temperature scans of the tensile modulus of the unfilled (unfilled circles) and the 10 wt% (filled circles) sample at (f = 10 rad/s, heating rate = 2 °C/min).

undeformed unfilled sample at room temperature is presented in Fig. 3(a). Deconvolution of the intensity profile into amorphous and crystalline components, as shown in Fig. 3(a), revealed the coexistence of α-monoclinic [34,35] and γ-triclinic [36–38] forms of isotactic polypropylene (iPP). The position of discrete reflections shown in Fig. 3 could be indexed as α(110)/γ(111) at $q = 10.2\ \mathrm{nm}^{-1}$, α(040)/γ(008) at $q = 11.8\ \mathrm{nm}^{-1}$, α(130) at $q = 13.0\ \mathrm{nm}^{-1}$, γ(117) at $q = 13.9\ \mathrm{nm}^{-1}$ and α(111)/γ(202) at $q = 15.1\ \mathrm{nm}^{-1}$. No discrete peaks were observed for the reflections α(13-1) and γ(026), which should appear at $q = 15.6$ and $15.7\ \mathrm{nm}^{-1}$, respectively. Therefore, these two peaks were not indexed, although they might still be present underneath the broad peak centered at $q = 15.1\ \mathrm{nm}^{-1}$. Moreover, it should be noted that the reflection: α(110)/γ(111) appeared as a shoulder rather than a strong narrow peak, in contrast with pure iPP crystals. As had been demonstrated [16] before, by increasing the ethylene portion of an EP copolymer, the α(110)/γ(111) reflection gradually weakened and progressively deviated from the pure iPP spectrum. Given that the crystals originated from the polypropylene chains, this behavior could be attributed to the amorphous phase that can be changed by controlling the non co-crystallizable ethylene segments.

The γ phase in random EP copolymers was first reported over three decades ago [39] and studied in detail by several groups [16,40]. It has been suggested [40] that the insertion of the comonomer units, such as ethylene, into an iPP chain reduces the length of the crystallizable sequence and promotes the formation of γ-crystals. It was experimentally observed [40] that the amount of γ-crystals was greatly affected by the ethylene content and reached a maximum value at about 15 wt% ethylene, which was close to the ethylene portion of EP copolymer chosen in this work.

Given that (1) several peaks of the α-form of iPP overlapped with peaks of the γ-form and (2) most reflection peaks were broad, a precise determination of their relative contributions to the total crystallinity index was out of reach. However, judging from the integrated area of γ(117) and of α(130) reflections, which did not overlap with any other, it was apparent in Fig. 3 that the nanocomposites had higher amounts of α crystals, when compared with those of the pure copolymer. In particular, with increasing MCNF loading (Fig. 3(b) 1 wt%, (c) 10 wt%, (d) 20 wt%), both the total crystallinity index, X_C^T, and the area ratio of α and γ crystalline peaks were increased, indicating that MCNF acted as a nucleation agent for the crystallization of the α-form iPP crystals in the EP copolymer matrix. Several studies [41–44] have clearly demonstrated that the incorporation of CNTs to the polypropylene matrix results in a faster crystallization rate and crystal growth. CNTs are known to promote the α-crystal formation in polypropylene, although the β-crystal formation has also been reported [41]. We did not find any corresponding studies in the literature for the EP copolymer thus far.

In the case of iPP with pronounced degree of stereo-irregularities, atomic force micrographs have shown [45] that the morphology obtained during crystallization contained α lamellae with epitaxial ongrowth of γ phase. If this picture were to hold true for the EP copolymer studied here, the presence of MCNFs seemed to disturb the ongrowth of γ phase by imposing steric constraints to its development, and thus decreased the total amount of γ crystallinity in the filled samples. One may also consider the higher thermal conductivity of the nanocomposite in comparison to the pure sample. Despite the fact that both filled and unfilled samples have been crystallized under identical conditions, i.e. quenched from melt to 0 °C (ice water) and isothermally crystallized at room temperature for several days, the effective temperature in the filled sample during quenching should be lower than the unfilled sample. Decreasing crystallization temperature is known to promote the nucleation of α crystals [45].

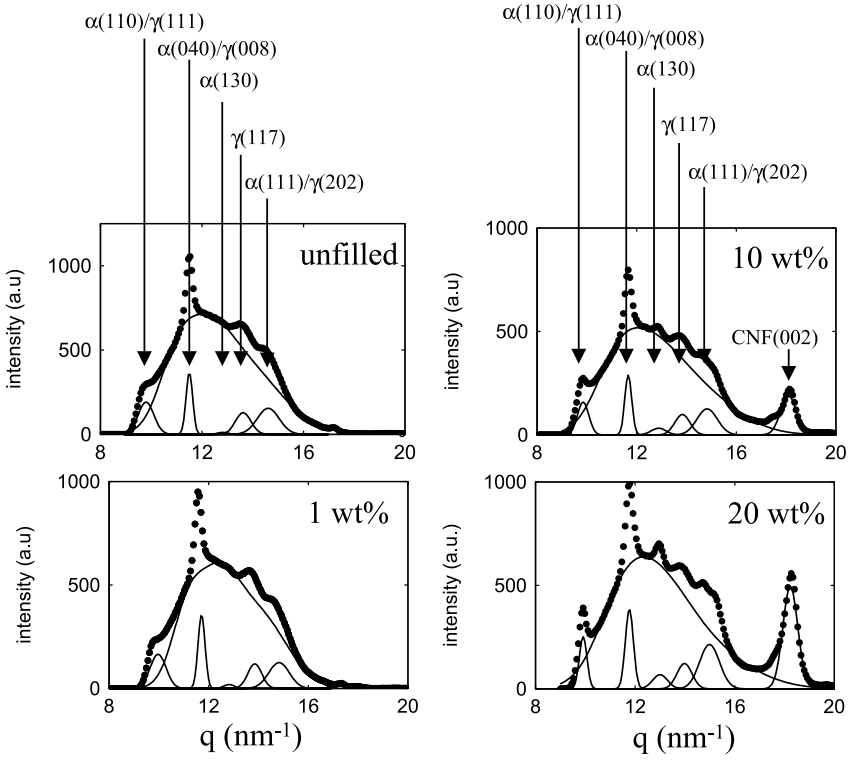

Fig. 3. Deconvolution of the circularly averaged WAXD intensity profiles into amorphous and crystalline components. The WAXD patterns were acquired at room temperature for the unstretched state of the samples; (a) unfilled, (b) 1 wt%, (c) 10 wt% and (d) 20 wt% filled nanocomposites.

4.3. In situ WAXD at room temperature

The stress–strain curves and selected WAXD patterns acquired during stretching at room temperature of the unfilled sample are compared with the corresponding data for the 10 wt% MCNF nanocomposite in Fig. 4. As expected, the patterns for the undeformed samples were isotropic, whereas those of the deformed samples were anisotropic, exhibiting more pronounced orientation at higher strains. The sharp isotropic diffraction rings in the WAXD patterns of the unstretched samples implied the presence of randomly distributed crystals. The presence of distinct diffraction arcs of the stretched samples was a common feature of the samples that exhibited a high degree of crystal orientation.

The obvious difference between the filled and unfilled samples was the presence of an outer ring ($q = 18.4\ \mathrm{nm}^{-1}$), as seen in the 10 wt% sample. This corresponds to a 3.4 Å spacing, which is consistent with the well studied [46–48] inter-shell spacing within the CNF structure (d_{002}); the Bragg peak that corresponds to d_{002} is referred as the (002) reflection of MCNF. It has been [47,48] shown that the inter-shell spacing in the CNTs is larger than that in pure graphite, indicating that CNTs have weaker van der Waals interactions between the adjacent graphitic layers. This has been attributed to the sharp curvature of the growing CNTs, which prevents the graphitic-like arrangements of the carbon atoms and facilitates the glide defects. In the glide

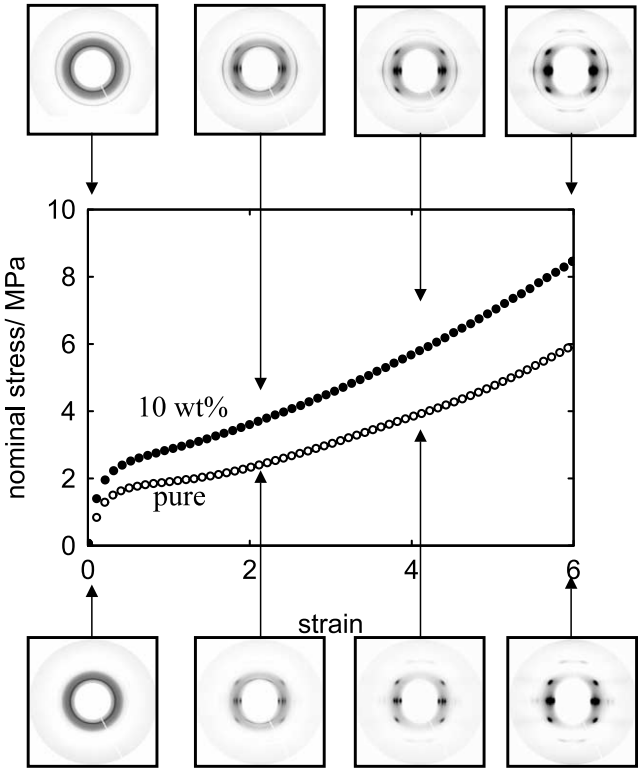

Fig. 4. Stress–strain curves and selected WAXD patterns acquired during stretching of pure copolymer (unfilled circles) and 10 wt% nanocomposite (filled circles) at room temperature.

defects, the concentric graphitic layers of CNFs slip with respect to one another so that the 100 planes become slightly titled. Therefore, this imperfect stacking (so called turbostratic [47]) is the origin of the more pronounced inter-shell separation observed in CNTs and CNFs in comparison with the pure graphite.

The circularly averaged WAXD intensity profiles for both unfilled and 10 wt% composite samples at several strains are presented in Fig. 5. Based on the integrated area ratio of γ(117) and α(130) peaks, it was seen that during stretching, the portion of the γ phase decreased in favor of the formation of α crystals. For the highly stretched samples (strain = 6), a small amount of γ crystallinity was still present in the filled sample, and even a lower amount (not quantified) in the unfilled sample. In general, martensitic [49,50] transformations, such as γ to α phase, can be generated by deformation through geometrical (steric) constraints involving structural rearrangements of neighboring chains. Martensitic transformations during stretching have been reported for several systems; in fact, they are quite common in alloys and steels, as well as in polymers. The transition of γ to α phase of isotactic polypropylene during stretching has been reported for poorly crystallized polypropylene materials with elastomeric behavior [51,52]. This phenomenon has been attributed to the non-parallel chain structure of the γ phase, in contrast with the parallel arrangement of the α phase. For the α phase, the succession of bilayers is such that the chain axes are parallel; whereas for the γ phase, the chain axes tilt ca. 81° with each other. The bilayers of γ phase cannot be completely aligned along the stretching direction; thus a large portion of the bilayers is placed almost normal to the stretching vector and is preferentially destroyed upon deformation.

In Fig. 6, the X_C^T value (derived from the integrated intensity profiles using the procedure described in Section 2) is plotted as a function of strain for pure copolymer and 10 wt% nanocomposite. At low strains, X_C^T is lower for the pure copolymer in comparison with the filled samples due to the nucleating effect of MCNFs. The X_C^T values of both samples increased at high strains, with X_C^T of the pure copolymer being seen to develop more rapidly and eventually overtaking the X_C^T value of the filled sample. The oriented and unoriented crystallinity indices (X_C^O and X_C^U respectively) for pure copolymer and 10 wt% nanocomposite are also plotted in Fig. 6. The destruction of some original crystals that took place at relatively low strains

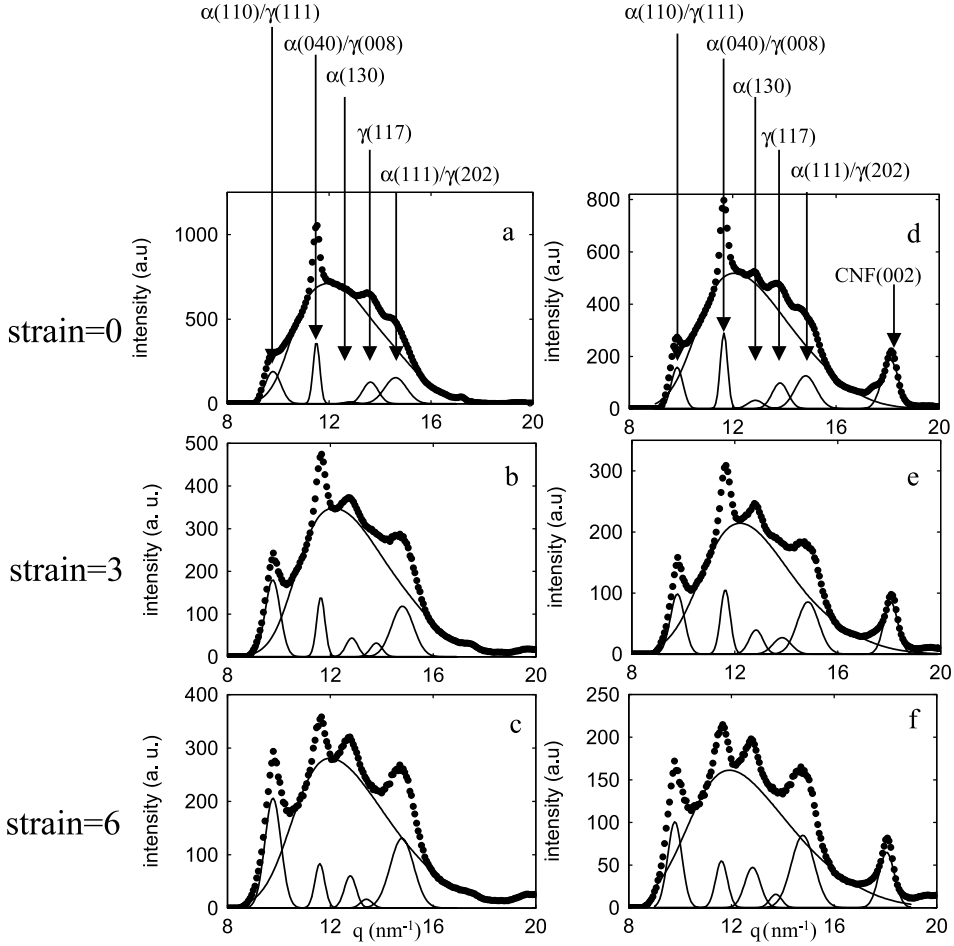

Fig. 5. Deconvolution of the circularly averaged WAXD intensity profiles into amorphous and crystalline components. The WAXD patterns were acquired during stretching at room temperature of pure copolymer ((a)–(c)) and 10 wt% nanocomposite ((d)–(f)). The corresponding strains are indicated.

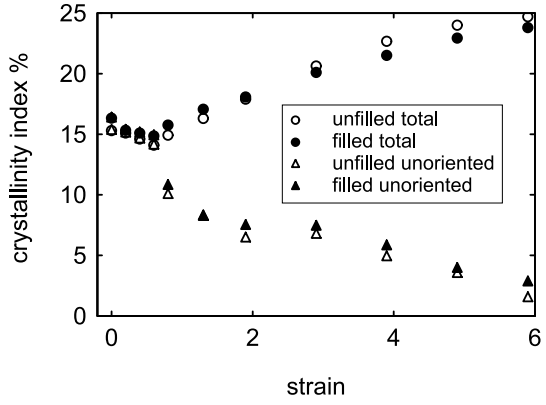

Fig. 6. Total (circles) and unoriented (triangles) crystallinity indices as a function of strain, determined during extension of pure copolymer (unfilled symbols) and 10 wt% nanocomposite (filled symbols) at room temperature.

('strain-induced melting' [53]) resulted in a decrease of X_C^T. Higher extensions led to the development of strain-induced crystallization. During elongation, the chains adopted extended conformations and tended to orient parallel to the stretching direction. Meanwhile, if a crystal experienced a stress that exceeded a critical value, it underwent a transition from the γ to the α phase.

At high strains, almost all the crystals were oriented in the pure copolymer, but some unoriented crystals were still present in the 10 wt% nanocomposite. In order to quantify the degree of crystal orientation along the stretching direction, we performed azimuthal scans at the α(040)/γ(008) peak position ($q = 11.8\ nm^{-1}$) of both filled and unfilled samples (Fig. 7(a)). The azimuthal profile was fitted with a Lorentzian function and its area was divided by the peak height to yield the integral breadth (IB). Fig. 7(b) illustrates the values of IB taken at the crystal α(040)/γ(008) reflection as well as at the (002) reflection of MCNF as a function of strain for both samples. It was seen that IB at the α(040)/γ(008) reflection decreased with strain for both samples, indicating an increase in the alignment of polymer crystals. Surprisingly, at the same strain, the polymer crystals of pure copolymer exhibited a higher degree of orientation than the filled sample, despite the fact that in the unfilled system, the stress was considerably reduced (Fig. 4). The IB value taken at the (002) reflection of MCNF also decreased with strain, indicating the improved MCNF alignment during stretching in the nanocomposite [54].

The highly stretched nanocomposite exhibited a higher amount of unoriented crystals and γ phase, as well as a lower degree of crystal orientation than the pure copolymer, indicated that the polymer crystals in the hybrid material experienced a reduced load. In other words, the load transfer from the matrix to MCNFs was rather efficient in the tested nanocomposite. Considering the following observations made in Figs. 4, 6 and 7: (1) the reinforcement effect of MCNFs increased with strain, and (2) X_C^T and the degree of orientation were higher in the unfilled sample than the filled sample at high strains; these findings can be attributed to the

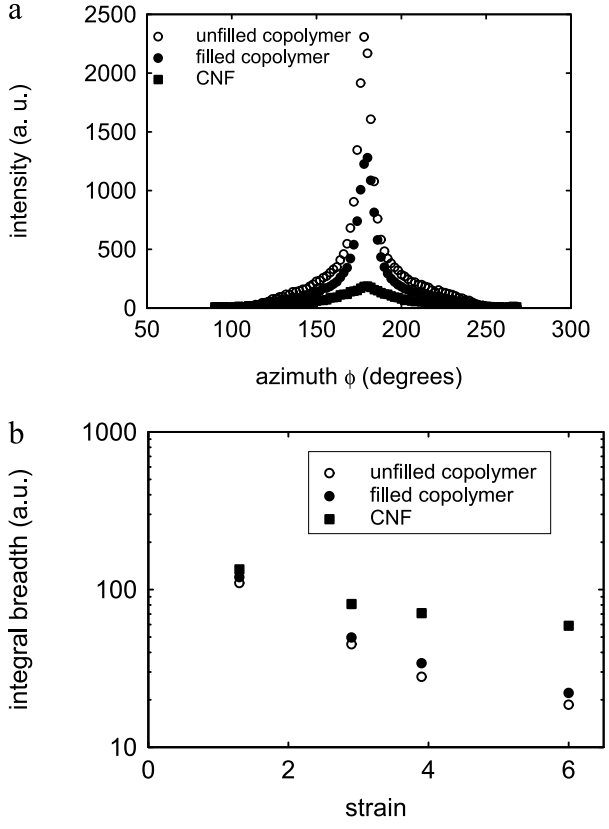

Fig. 7. (a) Azimuthal scans taken at the α(040)/γ(008) reflection of polymer crystals and the (002) reflection of MCNF obtained from the WAXD patterns of the filled and unfilled sample at stain = 6 at room temperature. (b) Integral breadth (IB) obtained from the azimuthal scans at varying strains. In (a) and (b), the circles (filled for the filled sample, open for the unfilled) correspond to the IB values taken at the α(040)/γ(008) reflection, the squares correspond to those taken at the (002) reflection of MCNF.

improved MCNF alignment along the stretching direction. In Fig. 7(b), the comparison of IB values taken at the α(040)/γ(008) reflection for iPP and the (002) reflection for MCNF indicates that the extent of MCNF orientation is considerably lower than the orientation of polymer crystals at the same strain. This behavior may be attributed to the relatively greater stiffness of MCNF in the nanocomposites than the polymer matrix.

Upon retraction, the orientation of the crystals and of MCNFs was reduced (Fig. 8). The amount of oriented crystals and the total crystallinity index, X_C^T decreased in filled and unfilled samples. However, they maintained higher values than those during extension at the same strain (Fig. 9), despite the fact that the stress during retraction was much smaller than the stress during extension. When the stress returned to zero, X_C^T was much higher than the original X_C^T value of the unstretched samples. The degrees of orientation for polymer crystals and MCNFs, as defined by the IB values, are plotted in Fig. 9(b). The degrees of orientation for both polymer crystals and MCNFs decreased upon retraction, but they remained higher than those observed at the same strain during extension.

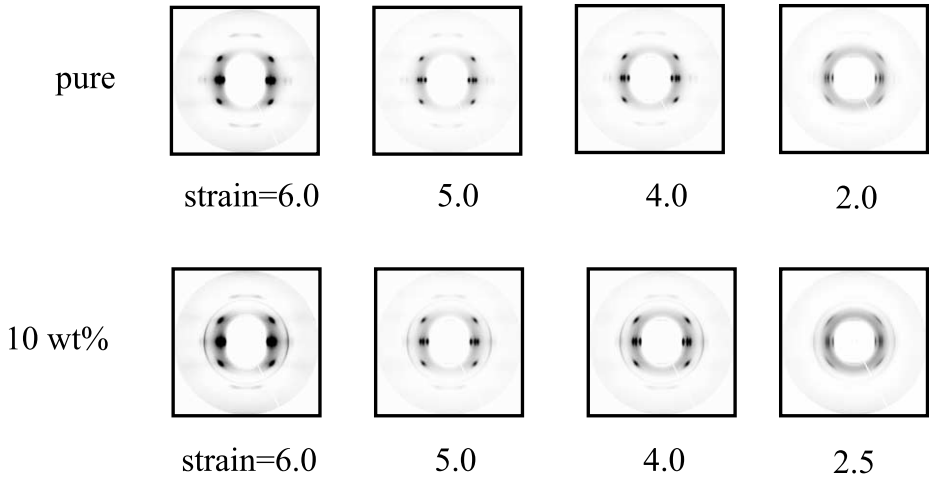

Fig. 8. WAXD patterns colleted during retraction at room temperature of (a) pure copolymer at and (b) 10 wt% filled sample at varying strains.

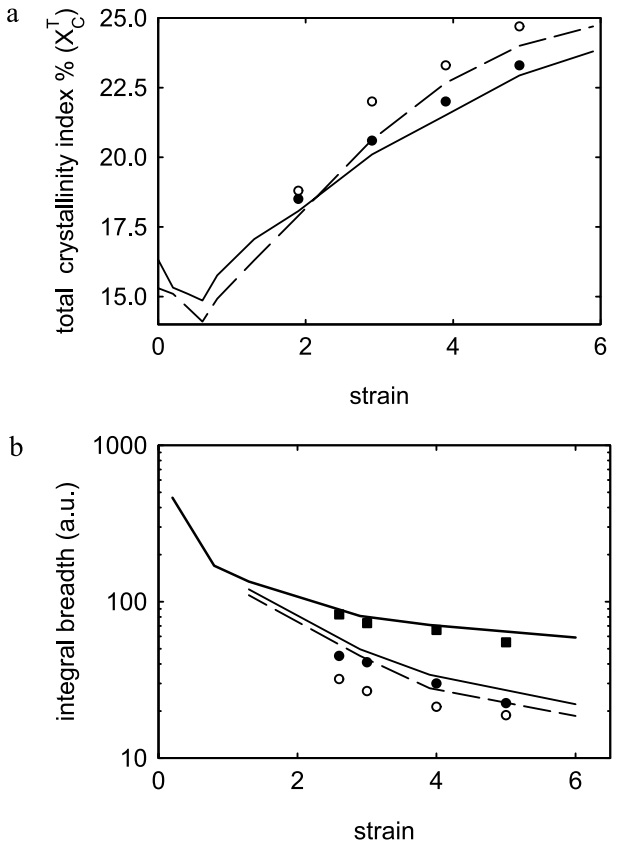

Fig. 9. (a) Total crystallinity index, X_C^T, as a function of strain determined during retraction of pure copolymer (unfilled symbols) and 10 wt% nanocomposite (filled symbols) at room temperature. The lines indicate the X_C^T value during extension of the neat polymer (dashed line) and the 10 wt% nanocomposite (full line). (b) Integral breadth (IB) plotted as a function of strain during retraction. The circles (filled for the filled sample, open for the unfilled sample) represent the IB values extracted from the α(040)/γ(008) reflection of polymer crystals, the squares correspond to those taken at the (002) reflection of MCNF. The lines indicate IB obtained during extension of pure copolymer (dashed line) and 10 wt% nanocomposite (thin line for the copolymer, thick line for MCNF).

For the unfilled copolymer, it has been shown [15] that zero stress after retraction coincides with zero orientation of the amorphous phase. This was also the case for the nanocomposite, which could be attributed to the following two reasons: (1) the polymer crystals exhibited a lower degree of orientation (in comparison with that of pure copolymer), and (2) the zero stress was reached at a higher strain in the nanocomposites. In Fig. 9(a), the lower values of X_C^T observed in the filled sample during retraction when compared with that in the unfilled sample was a consequence of the lower starting value of X_C^T. The amount of γ crystals was found to be about constant (very low) during retraction, indicating that the martensitic transformation from γ to α phase was an irreversible process, probably due to the higher thermodynamic stability of the α phase.

4.4. In situ WAXD at elevated temperatures

The stress–strain curves obtained at 55 °C for pure copolymer and 10 wt% nanocomposite are presented in Fig. 10. Both samples were stretched at a constant rate of 10 mm/min up to fracture. An increase in the tensile properties of the nanocomposites at 55 °C was, by far, more pronounced when compared with that at room temperature (Fig. 4); the toughness, i.e., the area under the stress-strain curve, was found to increase by a factor of 150 times in the 10 wt% filled sample than the unfilled one. Selected WAXD patterns of filled and unfilled samples during stretching are shown in Fig. 11. The deconvolution analysis indicated that partial melting of crystals took place in both unstretched samples, where the unfilled samples still contained the γ phase that appeared to be absent in the nanocomposites.

Fig. 12 illustrates the changes of X_C^T as a function of strain at 55 °C for filled and unfilled samples. Both samples underwent strain-induced melting at the initial stages of the drawing, but the filled sample retained a higher value of X_C^T at all strains due to the following synergistic effects: (1) the

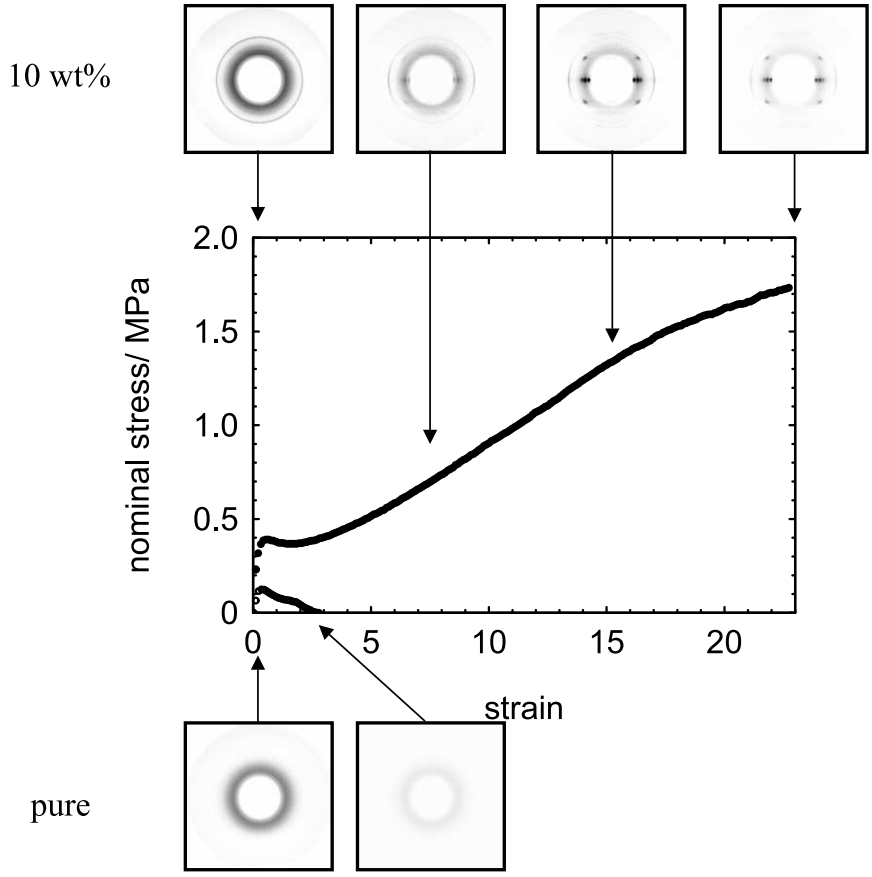

Fig. 10. Stress–strain curves and selected WAXD patterns acquired during stretching of the pure copolymer (unfilled circles) and 10 wt% nanocomposite (filled circles) at 55 °C.

higher initial crystallinity in the filled sample (as a result of the nucleating effect of MCNFs on the polymer matrix), (2) the absence of γ phase in the unfilled sample with the γ phase being known to be more sensitive to stretching, (3) the fact that nanofillers can induce a certain degree of polymer orientation, even in undeformed samples, leading to the development of thicker crystals that melt at higher temperatures than unoriented crystals, and (4) the reduced load experienced by the polymer matrix as demonstrated in Section 4.3. Such a 'reduced load effect' should be more efficient at higher temperatures, given that the crystals have more defects and, therefore, can be easily destroyed upon deformation.

Azimuthal scans (from 90 to 270°) taken at the (002) reflection of MCNF during stretching at 55 °C were analyzed to extract the degree of MCNF alignment at varying strains. In Fig. 13, IB obtained at 55 °C was compared with the data obtained at room temperature. It was found that the lower stress developed during extension at 55 °C resulted in a lower degree of alignment of MCNFs. At high strains, however, IB approached a plateau value, which coincided with the plateau value obtained during extension at room temperature. This plateau value might correspond to the maximum alignment of MCNFs that could be achieved during stretching of the tested nanocomposite.

The MCNF-reinforced polymer system exhibited decent tensile properties at high temperatures, e.g. the yield strength of about 0.1 MPa and the maximum elongation of about 800% at 60 °C (Fig. 14), while the tensile response of the pure copolymer was negligible at the same temperature. The drawability of the nanocomposite at high temperatures was significantly higher than that of the unfilled sample at the same temperature range. Fig. 15 illustrates the change of crystallinity during hot drawing for both filled and unfilled samples, which reflected the extent of structure development at high temperatures. The crystallinity development in the filled sample was quite significant even at 60 °C (Fig. 15(b)). At this temperature, the unfilled sample had very low X_C^T, beyond the detection limit of WAXD (Fig. 15(a)).

5. Discussion

5.1. Load transfer efficiency

As mentioned earlier, strong bonding in the MCNF–polymer interface is essential for the mechanical reinforcement of polymers. The efficient stress transfer from the polymer matrix to MCNFs in the present nanocomposite system is clear from the following observations:

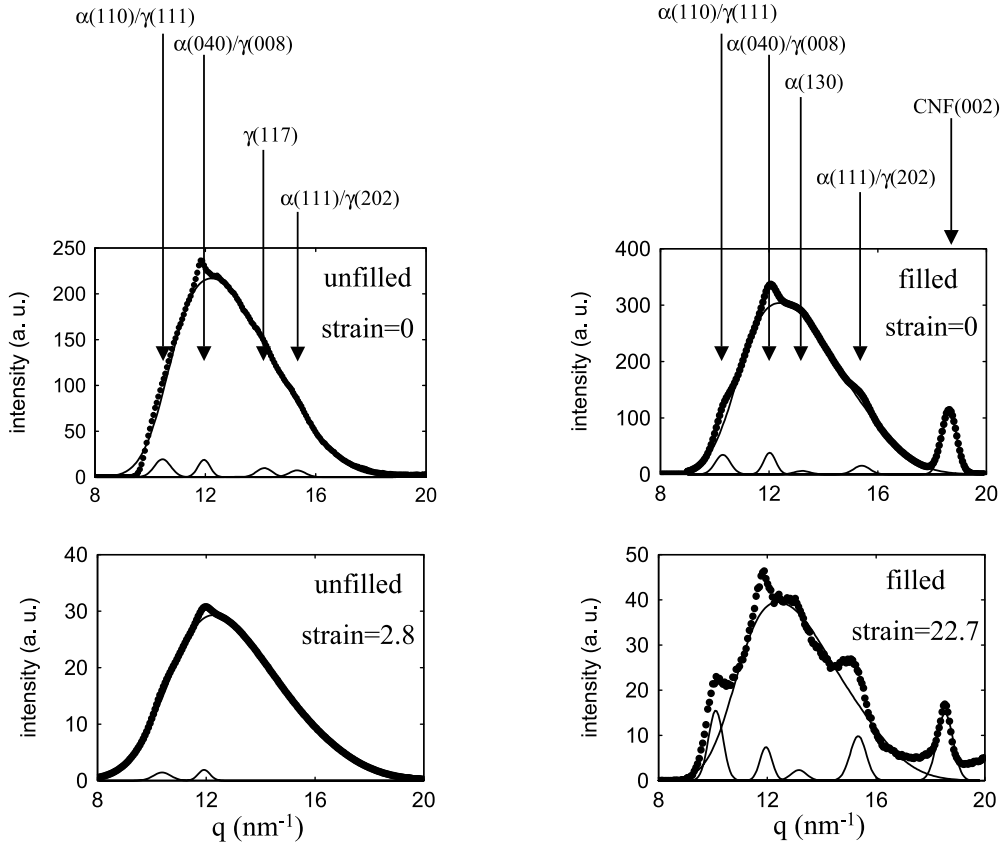

Fig. 11. Deconvolution of circularly averaged WAXD intensity profiles into amorphous and crystalline components. The patterns were acquired during stretching at 55 °C of the pure copolymer ((a) and (b)) and the 10 wt% nanocomposites ((c) and (d)). The strain was zero for (a) and (c), 2.8 for (b) and 22.7 for (d).

(1) As MCNF is an effective nucleating agent for the matrix, transcrystalline interface must be initiated on the surface of MCNFs. The presence of a crystalline polymer layer along the CNT can strongly enhance the load transfer [55]. Recently, a model that describes the composite reinforcement by considering the strength increase as a function of the thickness of the crystalline shell to the nanofiller surface has been proposed [56].

(2) The increased mechanical properties of the filled samples at room temperature in this study are direct proof of the efficient stress transfer from the matrix to MCNFs. The fact that at the same strain, a higher stress developed in the filled nanocomposites, but the amount of strain-induced crystallinity and the degree of polymer orientation was lower in the composite than

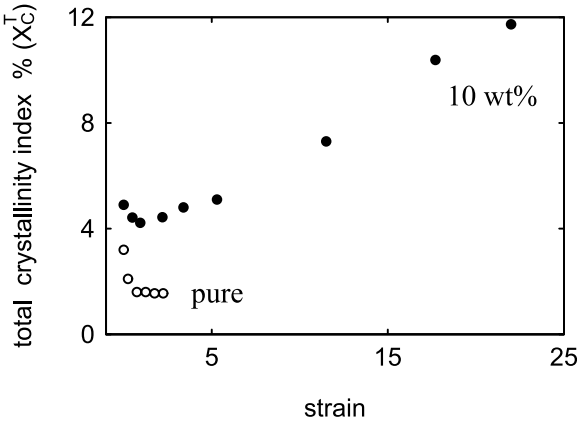

Fig. 12. Total crystallinity index, X_C^T, as a function of strain determined during extension of pure copolymer (unfilled symbols) and 10 wt% nanocomposite (filled symbols) at 55 °C.

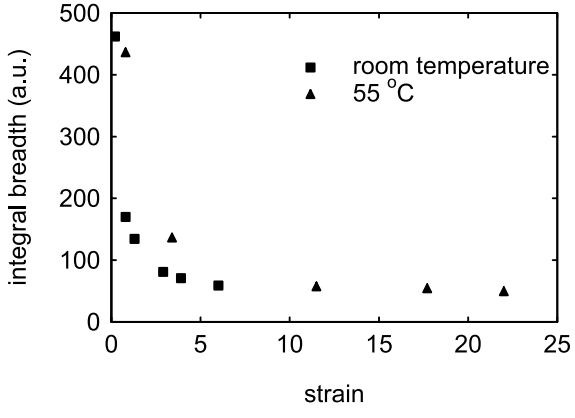

Fig. 13. Integral breadth (IB) obtained from the azimuthal scan at the (002) reflection of MCNF obtained from the 10 wt% nanocomposite during stretching at room temperature (squares) and at 55 °C (triangles). The data are plotted as a function of strain.

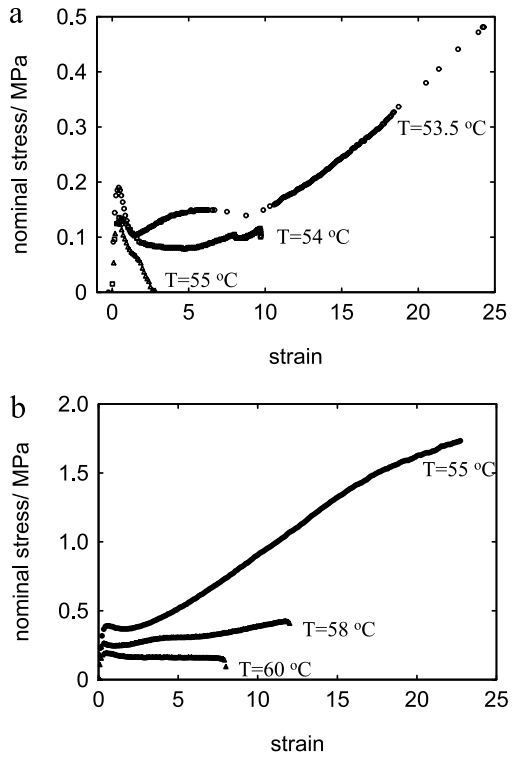

Fig. 14. Stress–strain curves of (a) pure copolymer and (b) 10 wt% nanocomposite at varying temperatures.

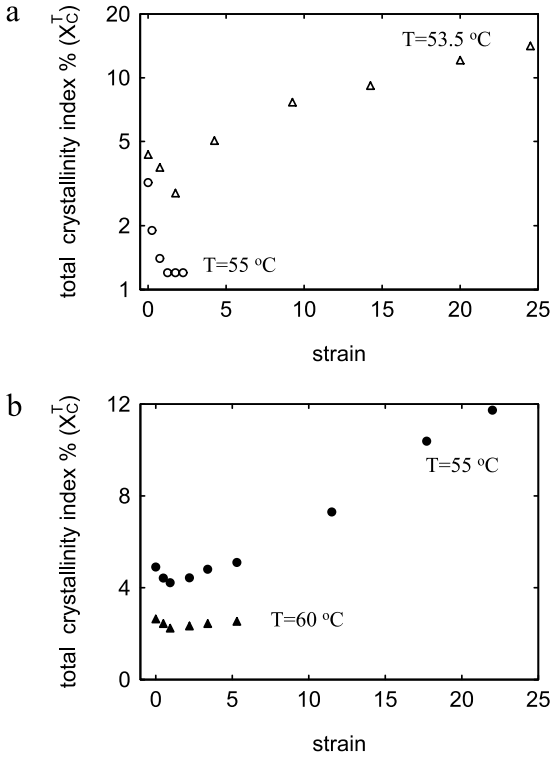

Fig. 15. Total crystallinity index, X_C^T, as a function of strain determined during extension of (a) pure copolymer and (b) 10 wt% nanocomposite at varying temperatures.

in the pure sample, indicating that the polymer matrix experienced a reduced stress as a result of efficient load transfer to MCNFs.

(3) The transformation of γ to α phase occurred at a certain critical stress and the observation that all of the γ phase in the pure copolymer was transformed to the α phase (Fig. 5) implied that the polymer matrix could experience a higher stress in the case of pure copolymer when compared with the filled sample (which contained a detectable amount of the γ phase). We conclude that MCNFs can successfully reduce the stress experienced in the bulk. This effect apparently increases the mechanical properties of the nanocomposite.

(4) Thermo-rheological properties of the nanocomposite and superior elastomeric performance at high temperatures, as clearly demonstrated in Figs. 2(b) and 10, respectively, could be attributed to a strong bonding in the MCNF–polymer interface. If this were not the case, agglomeration of MCNFs would take place at high temperatures, which would decrease the mechanical strength of the composite by creating low MCNF density areas. For example, in situ TEM observations during stretching [57] (in a MCNT–polystyrene system) showed that cracks appeared at low MCNT density areas and then propagated along the weak interfaces or low MCNT density regions. But this was not seen in this study.

In the case of CNT reinforced nanocomposites, Raman spectroscopy has been used to show that more efficient load transfer to the nanofiller takes place when the system is under compression rather than under tension [58]. This effect has been attributed to a pronounced slippage of the inner graphite layer with respect to the outer layer during stretching, whereas the possibility is minimized during compression due to geometrical constraints that the outer layers impose on the inner ones through buckling at the bent areas. The stiffness of the MCNTs used in this study, as revealed by the lower degree of orientation for MCNFs in comparison with the corresponding values of polymer crystals, led us to believe that the bending of MCNFs should not be pronounced during retraction. Based on the extent of orientation reported here for MCNF and polymer crystals, we assumed that the load transferring efficiency from the matrix to MCNFs was at about the same level during extension and compression.

The interfacial shear stress between the nanofiller and the matrix is a critical factor to determine the efficient load transfer. The chemical treatment of the surface of the nanofiller used here enhances the development of van der Walls interactions between the matrix and the MCNFs. Moreover, the grafted groups attached to the graphitic surface can promote the micromechanical interlocking of the matrix close to the MCNF surface, especially at elevated temperatures.

5.2. Stress–strain curves

In general, the stress–strain curves upon stretching of an elastomeric material above the glass transition temperature can be divided into five convenient subdivisions. (1) Zone I represents the elastic response of the system where the stress is a linear function of the strain. The crystallinity in this region is reduced due to 'strain-induced melting'. (2) Zone II represents the region where the rate of the stress increase is delayed as the system approaches the yield point. (3) Zone III shows where the stress decreases with strain, possibly due to a pronounced effect of crystal destruction rather than crystal development. (4) Zone IV shows the stress to reach a plateau value. This region of plastic resistance (so called the plastic flow region) is characterized by energy dissipated for the rearrangement, extension and orientation of the amorphous phase. (5) Zone V represents the region where the stress increases with strain almost linearly. This region corresponds to the upswing part of the stress–strain curve that is obtained before fracture. The strain-hardening region is dominated by the development of oriented crystals (strain-induced crystallization) and their perfection along the stretching direction.

The above features can be recognized in the plots displayed in Figs. 4 and 14. The absence of Zones III and IV in Fig. 4 is indicative of the rapid development of crystallinity under the chosen experimental conditions at room temperature. The absence of Zone V is apparent in the 54 and 55 °C plots of pure copolymer (Fig. 14(a)) and in the 58 and 60 °C plots of the 10 wt% nanocomposite (Fig. 14(b)). In these cases, the systems could not sustain significant deformation, due to the low viscosity and low effective entanglement density, as predicted by the classical rubber theory. According to the theory, the increase in temperature would decrease the modulus and, thus, the stress at all strains.

The deformation behavior of elastomeric ethylene/octene and ethylene/styrene copolymers at varying temperatures has been reported [59,60]. In general, the EP copolymer investigated in this study is consistent with the behavior observed in the above studies of different copolymers. The deformation behavior of ethylene–octene has been analyzed within the framework of the slip-link theory [59,60], in which the effects of two contributions: (1) the cross-link contribution and (2) the slip-link contribution, were considered. The cross-link contribution is due to the entanglements that become knotted upon stretching, resulting in a rigid mechanical response. The cross-links can coexist with slip-links, which can be visualized as the entanglements with ability to slide along the chain contour between the cross-links. Analytical deconvolution of the deformation curves leads to the conclusion that the effect of cross-links is independent of temperature at low and medium strains, in contrast with the slip-link effect, which increases with crystallinity and thus decreases with temperature. The slip-link contribution dominates at low and intermediate strains, and at low temperatures, whereas the cross-link contribution dominates at high temperatures and at high strains. Based on such an analysis, a mechanism for the crystal growth upon stretching has been proposed. This mechanism suggests the lateral attachment and detachment of chains at the crystal edges, which results in a topological constraint equivalent to a slip-link. Although this model was developed for the unfilled system, it might as well take place in the presence of MCNFs. In fact, the higher modulus at low strains (region dominated by slip-links) observed at room temperatures indicated that the presence of MCNFs enhanced this mechanism, e.g. by concentrating the crystals close to their surface or by orienting the detached chains to a nearby crystal. Moreover, taking into account that the incorporation of MCNFs resulted in higher modulus at all strains and at all the temperatures studied, we concluded that both cross-link and slip-link contributions are more pronounced in the nanocomposite than in pure copolymer.

It is seen that the incorporation of MCNFs enhances the mechanical properties of the composite at all temperatures, but the reinforcement is more pronounced at higher temperatures. This can be explained as follows. At room temperature, the presence of polymer crystals readily forms a physical network, where the addition of MCNFs generates an additional physical cross-linked network. Although the resulting morphology enhances the mechanical performance, the overall effect of MCNFs is only incremental not substantial. At elevated temperatures, as the crystallinity significantly decreases, the presence of MCNF in the nanocomposites can maintain the network structure, which is required to initiate the strain-induced crystallization, as seen in Fig. 10. The network formation of MCNF is thermally stable beyond the melting temperature of the matrix. For example, at 58 and 60 °C (Fig. 14), a long plastic flow region in Zone IV was seen, giving the composite very high drawability at temperatures where pure copolymer had negligible tensile performance.

In the absence of crystals, such as in a completely molten nanocomposite matrix, the long-range connectivity induced by nanofillers (e.g. MCNFs) can be monitored by the evolution of pseudo-gel like rheological response [61]. Within the linear viscoelastic region, these 'physical gels' [62] behave as 3D percolated networks, in which the macroscopic connectivity arises from polymer-filler interactions. In the particular case of the MCNF-EP nanocomposite studied here, an extensive investigation of the rheological response of its melt state showed pronounced deviations from the ideal melt behavior in the low frequency domain (positive slope of the tan $\delta(\omega)$ curves). This effect can be directly related to the physical cross-linking of MCNFs and will be discussed elsewhere [63]. In order to consider the physical cross-linking of MCNFs to the interpretation of the tensile experiments presented in this work we should consider the following two scenarios:

1. At low deformation strains, the presence of polymer crystals not only does not disturb, but actually enhances the long-range connectivity in the filled systems in comparison with the completely molten samples studied by rheology.
2. At high deformation strains, the reorientation of MCNFs preferentially along the stretching direction can destroy the connectivity of filler network in the other two dimensions. Nevertheless, the connectivity along the stretching direction is enhanced with strain.

In addition to the above arguments, the possibility of crystallographic deformation during stretching in the tested systems cannot be excluded. The plastic resistance of the (100)[001] chain slip in the α-crystals of iPP during biaxial deformation has been reported [64]. Thus, at elevated temperatures, the increased chain mobility due to partial melting and crystal defects induced by heating can facilitate the mechanism of chain slip. However, under the chosen experimental conditions, there was no evidence that this mechanism indeed took place. On the other hand, the destruction of the crystals (melting) at low strains, the martensitic transformation from γ to α iPP crystals, and the development of oriented crystallinity during stretching have been clearly seen in this study.

6. Conclusions

The MCNF-reinforced elastomeric EP copolymer studied here showed an advanced performance under uniaxial deformation and superior thermal stability. At room temperature, the EP copolymer crystallizes in a mixture of α and γ forms iPP crystals. We demonstrated that MCNF is an effective nucleating agent for iPP crystallization in EP copolymer. Upon stretching, the γ phase is preferentially destroyed in both filled and unfilled samples. The total crystallinity index, X_C^T, for both samples exhibits a minimum value due to (1) the initial strain-induced melting, and (2) the subsequent strain-induced crystallization. The higher maximum values of X_C^T and the higher degree of crystal orientation in conjunction with the lower amount of γ crystals, observed in the stretched unfilled sample, are consistent with the development of higher effective stress in the unfilled system. This indicates that, at room temperature, the polymer matrix in the nanocomposite experienced a reduced stress, as a result of efficient load transfer from the polymer matrix to MCNFs. Deformation at elevated temperatures showed a significant MCNF reinforcement effect on the properties of partially melted matrix. In this case, the presence of MCNF provides a physical cross-linking network to the matrix, which facilitates the strain-induced crystallization. The combined effects significantly enhance the mechanical properties of the nanocomposites.

Acknowledgements

The financial support of this work was provided by the Office of Naval Research (N000140310932) and the National Science Foundation (DMR-0405432). The authors acknowledge the assistance of Dr Lixia Rong for synchrotron WAXD experimental setup.

References

[1] Baughman RH, Zakhidov AA, de Heer WA. Science 2002;297:787.
[2] Kashiwagi T, Grulke E, Hilding J, Groth K, Harris R, Butler K, et al. J Polym 2004;45:4227.
[3] Qian D, Dickey EC, Andrews R, Rantell T. Appl Phys Lett 2000;76:2868.
[4] Schadler LS, Giannaris SC, Ajayan PM. Appl Phys Lett 1998;73:3842.
[5] Biercuk MJ, Llaguno MC, Radosavljevic M, Hyun JK, Johnson AT, Fischer JE. Appl Phys Lett 2002;80:2767.
[6] Baughnam RH, Cui C, Zakhidov AA, Iqbal Z, Barisci JN, Sprinks GM, et al. Science 1999;284:1340.
[7] Iijima S. Nat (London) 1991;354:56.
[8] Andrews R, Weiseberger MC. Curr Opin Solid State Mater Sci 2004;8:31.
[9] Star A, Stoddart JF, Steuerman D, Diehl M, Boukai A, Wong EW, et al. Angew Chem, Int Ed 2001;40:1721.
[10] Lordi V, Yao N. J Mater Res 2000;15:2770.
[11] Hirsch A. Angew Chem, Int Ed 2002;41:1853.
[12] Sun Y-P, Fu K, Lin Y, Huang W. Acc Chem Res 2002;35:1096.
[13] Niyogi S, Hamon MA, Hu H, Zhao B, Bhowmik P, Sen R, et al. Acc Chem Res 2002;35:1105.
[14] Blake R, Gunko YK, Coleman J, Cadek M, Fonseca A, Nagy JB, et al. J Am Chem Soc 2004;126:10226.
[15] Toki S, Sics I, Liu L, Hsiao BS, Tsou AH, Datta S. Am Chem Soc Rubber Div Prepr 2003;2055.
[16] Datta S, Srinivas S, Cheng CY, Tsou A, Lohse DJ. Rubber World 2003;229:55.
[17] Rodriguez NM. J Mater Res 1993;8:3233.
[18] http://www.apsci.com/ngm-pyro1.html. Information about the CNF-modulus.
[19] Lozano K, Barrera EV. J Appl Polym Sci 2000;79:125.
[20] Kumar S, Doschi H, Srinivasarao M, Park JO, Schiraldi DA. Polymer 2002;43:1701.
[21] Finegan IC, Tibbetts GG, Glasgow DG, Ting J-M, Lake ML. J Mater Sci 2003;38:3485.
[22] Ran S, Burger C, Sics I, Yoon K, Fang D, Kim K, et al. Colloid Polym Sci 2004;282:802.
[23] Kharchenco SB, Douglas JK, Obrzut J, Grulke EA, Migler KB. Nat Mater 2004;3:564.
[24] Frogley MD, Ravich D, Wagner HD. Compos Sci Technol 2003;63:1647.
[25] Koerner H, Price G, Pearce NA, Alexander M, Vaia RH. Nat Mater 2004;3:115.
[26] Eitan A, Jiang K, Dukes D, Andrews R, Schadler LS. Chem Mater 2003;15:3198.
[27] Lim J, Yun W, Yoon M, Lee SK, Kim C, Kim K, et al. Synth Met 2003;139:521.
[28] Hu H, Bhowmik P, Zhao B, Hamon MA, Itkis ME, Haddon RC. Chem Phys Lett 2001;345:25.
[29] Oh SJ, Jung JC, Zin W-C. J Colloid Interf Sci 2001;238:43.
[30] Fraser RDB, MacRae TP, Millar A, Rowlands RJ. J Appl Cryst 1976;9:81.

[31] Ran S, Zong X, Fang D, Hsiao B, Chu B, Ross R. J Appl Crystallogr 2000;33:1031.
[32] Wei ZG, Sandstrorom R, Miyazaki S. J Mater Sci 1998;33:3743.
[33] Wei ZG, Sandstrorom R, Miyazaki S. J Mater Sci 1998;33:3763.
[34] Nogales A, Hsiao BS, Somani RH, Tsou AH, Balta-Calleja FJ, Ezquerra TA. Polymer 2001;42:5247.
[35] Somani RH, Yang L, Hsiao BS, Agarwal PK, Fruitwala HA, Tsou AH. Macromolecules 2002;35:9096.
[36] Brucker S, Philips PJ, Mezghani K, Meille SV. Macromol Rapid Commun 1997;18:1.
[37] Perez E, Zucchi D, Sacchi MC, Forlini F, Bello A. Polymer 1999;40: 675.
[38] Thomann R, Semke H, Maier R-D, Thomann Y, Scherble J, Mulhaupt R, et al. Polymer 2001;42:4597.
[39] Turner-Jones A. Polymer 1971;12:487.
[40] Feng Y, Jin X, Hay JN. J Appl Polym Sci 1998;68:381.
[41] Grady BP, Pompeo F, Shambaugh RL, Resasco DE. J Phys Chem B 2002;106:5852.
[42] Bhattacharyya AP, Sreekumar TV, Liu T, Kumar S, Ericson LM, Hauge, Hauge RE. Polymer 2003;44:2373.
[43] Assouline E, Lustiger A, Barber AH, Cooper CA, Klein E, Wachtel E, et al. J Polym Sci, Part B: Polym Phys 2003;41:520.
[44] Valentini L, Biagiotti J, Kenny JM, Santucci S. Compos Sci Technol 2003;63:1149.
[45] Thomann R, Semke H, Maier R-D, Thomann Y, Scherble J, Mulhaupt R, et al. Polymer 2001;42:4597.
[46] Zhou O, Fleming RM, Murphy DW, Chen CT, Haddon RC, Ramirez AP, et al. Science 1994;263:1744.
[47] Sum X, Kiang C-H, Endo M, Takeuchi K, Furuta T, Desselhaus MS. Phys Rev B 1996;54:R12629.
[48] Endo M, Takeuchi K, Hiraoka T, Furuta T, Kasai T, Sun X, et al. J Chem Solids 1997;58:1707.
[49] Lotz B, Mathiou C, Thierry A, Lovinger AJ, De Rosa C, Ruiz de Ballesteros O, et al. Macromolecules 1998;31:9253.
[50] Auriemma F, De Rosa C. J Am Chem Soc 2003;125:13143.
[51] Auriemma F, De Rosa G, Boscato T, Corradini P. Macromolecules 2001;34:4815.
[52] De Rosa C, Auriemma F, Perretta C. Macromolecules 2004;37:6843.
[53] Liu L-Z, Hsiao BS, Fu BX, Ran S, Toki S, Chu B, et al. Macromolecules 2003;36:1920.
[54] Jin L, Bower C, Zhou O. Appl Phys Lett 1998;73:1197.
[55] Cadek M, Coleman JN, Barron V, Hedicke K, Blau W. J Appl Phys Lett 2002;81:5123.
[56] Coleman JN, Cadek M, Blake R, Nicolosi V, Ryan KP, Belton C, et al. Adv Funct Mater 2004;14:791.
[57] Qian D, Dickey EC, Andrews R, Rantell T. Appl Phys Lett 2000;76: 2868.
[58] Schadler LS, Giannaris SC, Ajayan PM. Appl Phys Lett 1998;73: 3842.
[59] Bensason S, Stepanov EV, Chum S, Hiltner A, Baer E. Macromolecules 1997;30:2436.
[60] Chang A, Cheung YW, Hiltner A, Baer E. J Polym Sci, Part B: Polym Phys 2001;40:142.
[61] Mitchell CA, Bahr JL, Arepalli S, Tour JM, Krishnamoorti R. Macromolecules 2002;35:8825.
[62] Horst RH, Winter HH. Macromolecules 2000;33:30–136.
[63] Kelarakis A, Yoon K, Somani R, Hsiao BS, Chu B. Unpublished.
[64] Bartczak Z, Galeski A. Polymer 1999;40:3677.